Ionics (2019) 25:5709–5716
https://doi.org/10.1007/s11581-019-03107-0

ORIGINAL PAPER

Synthesized Fe-doping $Li_3V_2(PO_4)_3$/C cathode material from combustion synthesis precursors with enhanced electrochemical performance

Zhiqin Cao[1] · Chengyang Zuo[1] · Xumei Cui[1] · Xuefeng Zhang[1]

Received: 8 April 2019 / Revised: 16 May 2019 / Accepted: 3 June 2019 / Published online: 10 July 2019

Abstract

Fe-doping $Li_3V_2(PO_4)_3$/C material was successfully synthesized from combustion synthesis precursors. The $Li_3V_2(PO_4)_3$ is layered by amorphous carbon with a porous structure and doped with Fe, which can improve the Li^+ transfer rate and conductivity. The 1% Fe-doped products used as cathode electrode for lithium-ion batteries exhibit enhanced electrochemical performance. In 3.0~4.8 V, it has a specific discharge capacity of 180 mAh g^{-1} after 20 cycles at 0.1 C, 142.5 mAh g^{-1} after 500 cycles at 1 C, and 132.5 mAh g^{-1} after 500 cycles at 10 C. Moreover, it shows stabilized specific discharge capacity of 65.9 mAh g^{-1} after 500 cycles at a rate of 20 C, and the capacity retention is 98%. Thus, it could infer the Fe-doping $Li_3V_2(PO_4)_3$/C material is a permission candidated material for application in lithium-ion batteries with high performance.

Keywords Solution combustion synthesis · $Li_3V_2(PO_4)_3$ · Cathode · Electrochemical performance

Introduction

Lithium-ion batteries (LIBs) employed in hybrid electric vehicle energy storage device have been attracting great attention for their light weight, high safety, high energy, and long cycle durability without a memory effect [1, 2]. To develop desired electrode materials with high performance including excellent rate capability, high reversible discharge capacity and cycle stability are crucial for LIBs, especially for cathode materials [2, 3]. In recent decades, in order to achieve the increasing demand performance, various kinds of cathode materials have been researched and developed, such as lithium transition-metal phosphates. Due to the good structural stability, high theoretical specific capacity, and operating voltage [4, 5], lithium transition-metal phosphates have attracted significant attention in LIBs with high performance. Among the transition-metal phosphate compounds, $Li_3V_2(PO_4)_3$ (monoclinic) is the most prospective material ascribed to its acceptable ionic mobility, high theoretical specific capacity, operating voltage, and thermodynamically stable structure [6, 7]. However, the separated [VO_6] octahedral arrangements result in the poor electronic conductivity of $Li_3V_2(PO_4)_3$ (2.4–10^{-7} S cm^{-1}), which indeed limits its extensive application [8, 9]. Great efforts have been devoted to resolve those problems, such as coating $Li_3V_2(PO_4)_3$ with a carbon layer [10, 11], reducing its particle size [12, 13] and cation doping [14, 15]. Among them, cation doping is a facility and effective method to enhance the electrochemical properties of $Li_3V_2(PO_4)_3$ [16]. Up to now, a great number of cations, such as Zr^{3+}, Mn^{2+}, Al^{3+}, Cu^{2+}, Mg^{2+}, Fe^{3+}, Ge^{4+}, and Cr^{3+} have been employed as dopants for $Li_3V_2(PO_4)_3$ and achieved some good results [14–20].

Previously, several methods have been adopted to synthesize cation doping $Li_3V_2(PO_4)_3$, which include hydrothermal technique, spray pyrolysis method, solid-state strategy, and sol-gel approach. For example, Park et al. [19] have prepared Mn-doping $Li_3V_2(PO_4)_3$ by the spray pyrolysis method. The electric conductivity of $Li_3V_2(PO_4)_3$ has been increased ascribed to the Mn doping, and the cathode electrode performances have been improved. Liu et al. [20] used two methods (the first step is the sol-gel method) to fabricate Fe-doping $Li_3V_2(PO_4)_3$ with improvement of electrochemical performance. However, these methods usually consist of redundant steps, such as a long time for reaction, washing several times, and calcination at various stages to prepare the final product.

✉ Zhiqin Cao
cao_zhi_qing@163.com

[1] College of Vanadium and Titanium, Panzhihua University, Panzhihua 617000, China

Thus, it is valuable to develop a facile synthesis route with low cost and efficiency for practical application. Up to now, we find no literature report on the preparation of Fe-doped LVP by combustion synthesis. In this work, we offer a facile route for the synthesis of Fe-doping $Li_3V_2(PO_4)_3$ using solution combustion synthesis. Compared with conventional synthesis methods, this method (solution combustion synthesis) is effective and economic due to time-saving processing and economic and simple experimental set-up [21–23]. Electrochemical measurement results imply the as-prepared Fe-doping $Li_3V_2(PO_4)_3$ is a permission candidated cathode material for application in lithium-ion batteries with high performance.

Experimental

Synthesis

In detail, 0.03 mol lithium nitrate ($LiNO_3$), 0.02 mol ammonium metavanadate (NH_4VO_3), 0.02 mol ammonium dihydrogen phosphate ($NH_4H_2PO_4$,), ferric nitrate ($Fe(NO_3)_3 \cdot 9H_2O$), 2 g glucose ($C_6H_{12}O_6 \cdot H_2O$,), and 0.07 mol glycine (NH_2CH_2COOH) were dissolved in 200 ml deionized water. All the chemicals were analytical reagent grade (Shanghai Zhanyun Chemical Co., Ltd.). The ratio between Fe and $Li_3V_2(PO_4)_3$ (0.02 mol ammonium metavanadate could prepare 0.01 mol $Li_3V_2(PO_4)_3$) was 0~2 (wt%). The whole process for preparation precursors takes 15–20 min. Then, the precursors prepared by combustion synthesis were heated at 800 °C for 5 h with N_2 atmosphere, and then Fe-doping $Li_3V_2(PO_4)_3$ could be gotten.

Characterizations

The prepared samples were characterized with X-ray diffraction (XRD, MXP21VAHF) at room temperature, X-ray photoelectron spectra (XPS, PerkinElmer), scanning electron microscopy (SEM), and transmission electron microscopy (TEM).

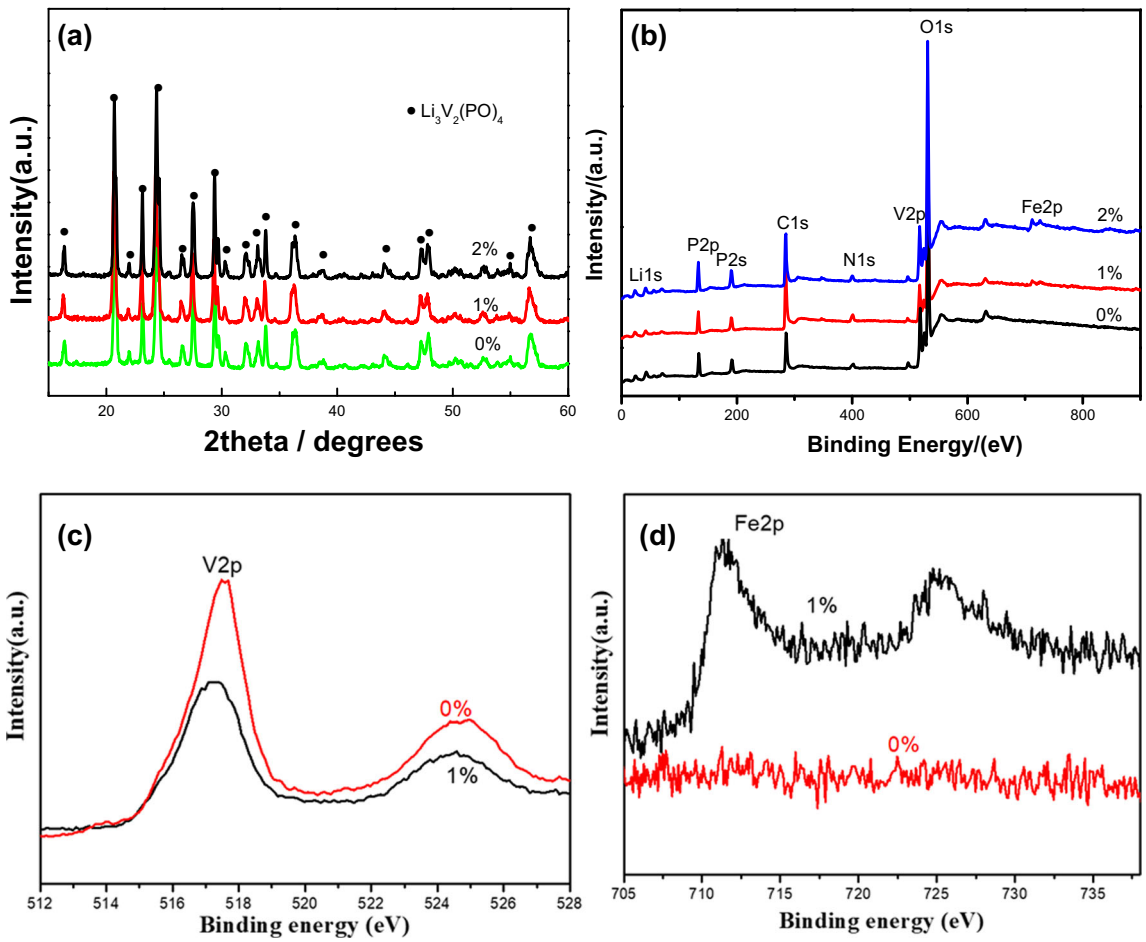

Fig.1 **a** XRD patterns of the $Li_3V_2(PO_4)_3$/C samples with the different Fe contents. **b** Survey XPS spectra of samples, high-resolution XPS analysis of **c** V2p and **d** Fe2p for 0 wt% and 1 wt% samples

Electrochemical measurements

The electrodes were fabricated by a mixture of Fe-doping $Li_3V_2(PO_4)_3$ materials (80 wt%), acetylene black (10 wt%), and poly (10 wt%). The compounds were scattered in N-methyl-2-pyrrolidone (NMP) to form sizing agent, depositing on an Al foil. All the fabricated electrodes were stoved at 80 °C for 10 h in a vacuum oven. The half cells (CR2032-type) were fabricated in an Ar-filled glove box. The electrolyte was a non-aqueous solution with 1 M $LiPF_6$ dissolved in a mixture of 1:1:1 of ethylene carbonate (EC)/dimethyl carbonate (DMC)/ethylene methyl carbonate (EMC). The charge and discharge properties of the cells with different current densities were tested in 3.0–4.8 V. For the capacity rate testing, the current gradually changed from 0.5 to 1, 2, 5, and 10 C and decreased to 0.5 C. Cyclic voltammetry (CV) curves were studied with CHI710D (Chenhua, Shanghai) electrochemical workstation at the rate of 0.1 mV s^{-1}.

Results and discussion

Figure 1a demonstrates the XRD results of the as-prepared products. All diffraction peaks can be labeled as the crystalline monoclinic $Li_3V_2(PO_4)_3$ (JCPDS 97-009-6962), and no other peaks could be found. It indicated the $Li_3V_2(PO_4)_3$ has been successfully prepared by reduction combustion synthesis precursors at a temperature of 800 °C for 5 h. Figure 1b shows the chemical information of samples characterized by XPS. According to Fig. 1b, the Li, P, C, V, O, N, and Fe elements could be found. The ~ 55.7 eV band is due the contribution of Li^+ in $Li_3V_2(PO_4)_3$ [24]. The ~ 140 eV band is attributed to 2P3/2 in $(PO_4)_3$ [25]. The peak at 531.5 eV was the O1s spectrum generated by $(PO_4)_3$ [26]. The peak located at

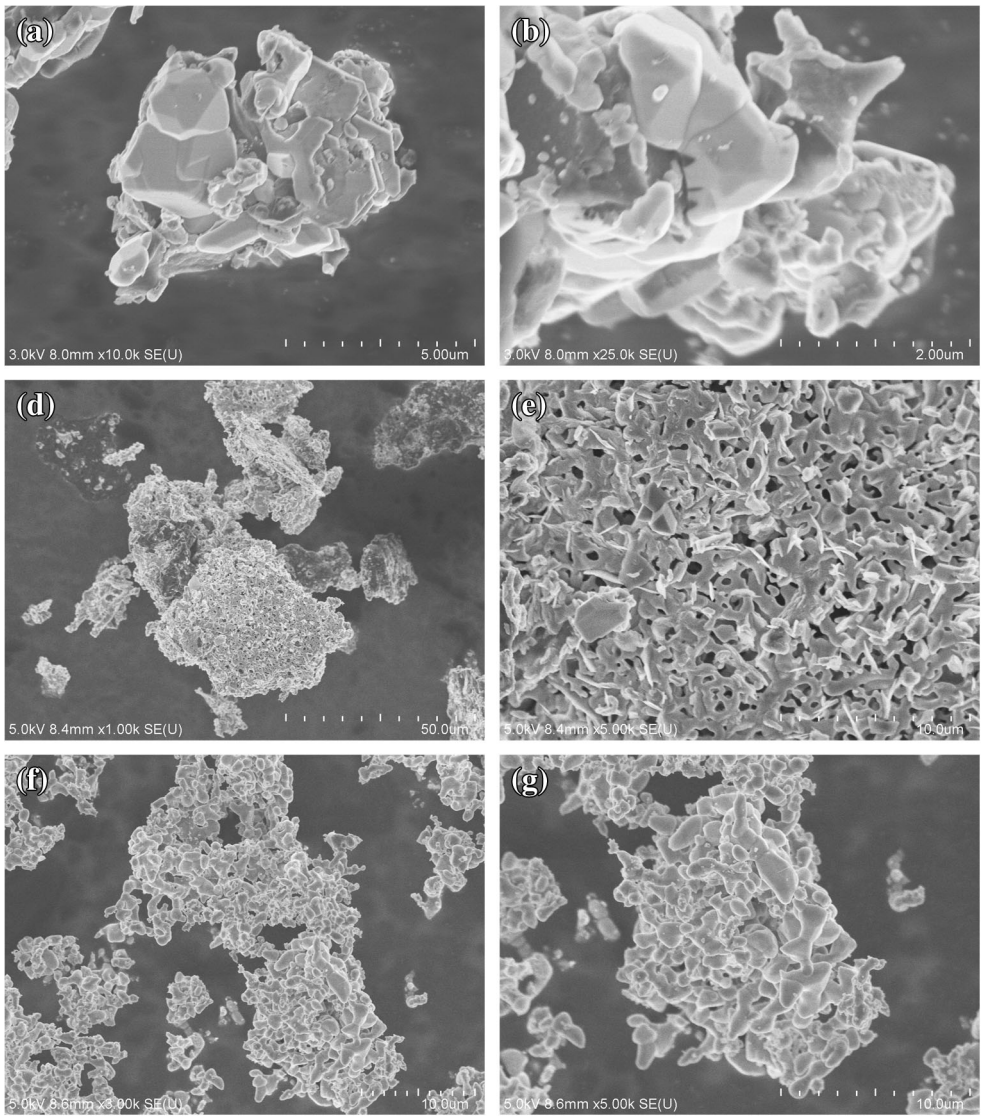

Fig. 2 SEM images of the $Li_3V_2(PO_4)_3$/C samples with the different Fe contents. **a**, **b** 0%. **c**, **d** 1%. **e**, **f** 2%

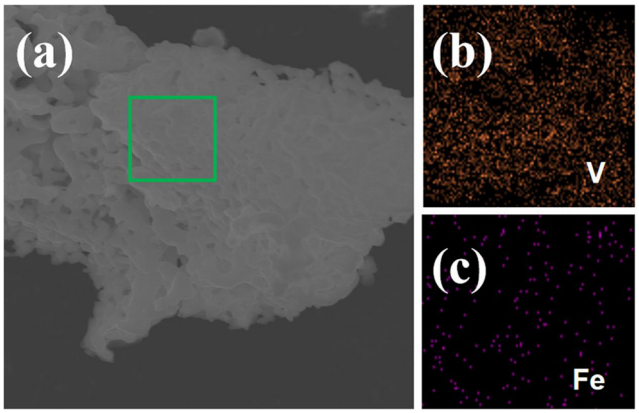

Fig. 3 **a** Original SEM images of 1% Fe-doped $Li_3V_2(PO_4)_3$/C powders and **b** V and **c** Fe map distribution

285 eV is corresponding C1s in carbon [27]. The ~400 eV peak confirms the N1s in samples [28]. In the high-resolution XPS of V2p for 0 wt% and 1 wt% samples, as shown in Fig.1c, the V2p with a binding energy of around 517 eV ascribed to V2p, which correspond to V^{3+} in $Li_3V_2(PO_4)_3$ [29]. Additionally, the high-resolution XPS of Fe2p for 0 wt% and 1 wt% samples are shown in Fig.1d. It can be found that new peaks of Fe2p with a binding energy around 711 eV [30] appeared in the Fe-doped sample and no characteristic peak of Fe in 0% sample. The XPS results indicate the Fe-doped $Li_3V_2(PO_4)_3$ has been successfully prepared.

Figure 2 illustrates the SEM characterizations of all samples. As illustrated in Fig.2, the 0% sample and 2% sample has a bulk structure and composed of irregular

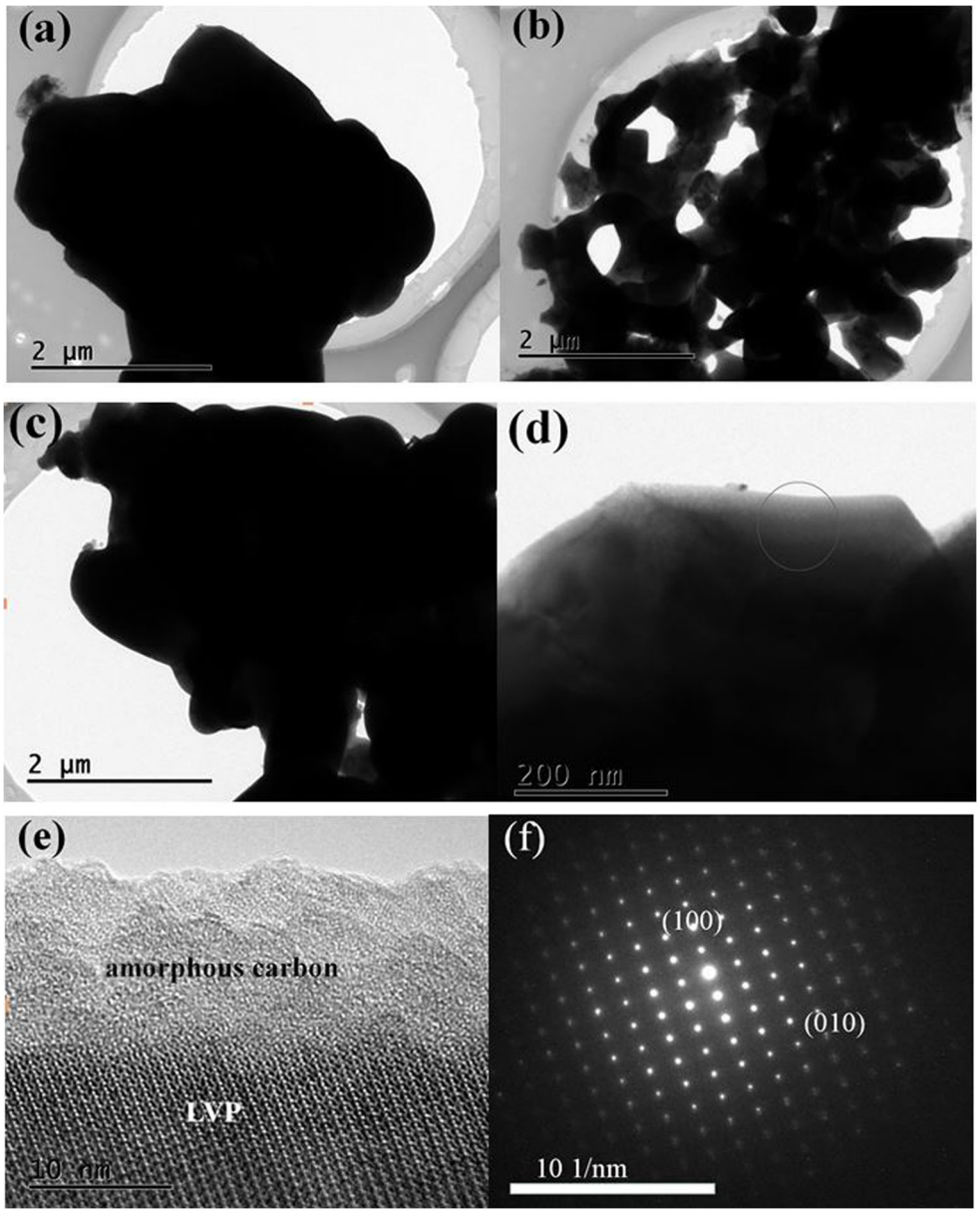

Fig. 4 TEM images of the $Li_3V_2(PO_4)_3$/C samples with the different Fe contents. **a** 0%. **b** 1%. **c** 2%. **d**–**f** HR-TEM of $Li_3V_2(PO_4)_3$/C with Fe content of 1%

particles. The 1% sample has a porous structure and composed of a sheet structure, which is favorable for lithium ion transmission [31]. By comparison, the Fe-doped $Li_3V_2(PO_4)_3$ have less agglomeration than pure $Li_3V_2(PO_4)_3$, particularly for the 1% sample. This is due to the Fe source (ferric nitrate) which was added in the sample. In this work, it used solution combustion method (SCS) to synthesize precursors. For the SCS, ferric nitrate is the oxidant in the system. When ferric nitrate was induced in the system, the precursors were prepared by the reaction, and the ratio of fuel and oxidant was increased. It could affect the chemical energy and gases liberated in the reaction process [32, 33]. Because of the dispersant effect of more gases on the products [34], the 1% sample has a porous structure. When the Fe content was added to the 2% sample, the surpassing oxidation in the reaction system and the surpassing energy generated in the system, and the particles began to grow and agglomerated. So, the morphology of the product has been changed. Figure 3 exhibits the original images of 1% Fe-doped $Li_3V_2(PO_4)_3$/C powders and the map distribution of V and Fe elements. It is visible in Fig. 3b that the powders have homogeneous distribution of V and Fe elements. Because all raw materials were dissolved in water, all elements in the reaction system uniformly mixed at a molecular or atomic level. And the elements in the samples could distribute homogeneously.

To further observe the structure and morphology of the products, TEM images of pure and Fe-doping $Li_3V_2(PO_4)_3$ products are displayed in Fig. 4. It is clear that pure $Li_3V_2(PO_4)_3$ (Fig. 4a) and 2% Fe-doping $Li_3V_2(PO_4)_3$ (Fig. 4c) have a bulk structure, and the 1% Fe-doped $Li_3V_2(PO_4)_3$ (Fig. 4b) shows a highly porous structure with interconnected macropores. High-resolution transmission electron microscope (HRTEM) investigations of 1% Fe-doped $Li_3V_2(PO_4)_3$ (Fig. 4d–f) demonstrate the modified $Li_3V_2(PO_4)_3$ are covered with amorphous carbon, which can improve the electron conductivity of the products. To study the crystalline nature of $Li_3V_2(PO_4)_3$, electron diffraction of $Li_3V_2(PO_4)_3$ was performed. Figure 4f exhibits the selected electron diffraction pattern, and the distinctive diffraction patterns confirm the highly crystalline nature of the 1% Fe-doped $Li_3V_2(PO_4)_3$. The clear diffraction spots further represent the monoclinic crystal system of $Li_3V_2(PO_4)_3$ phase which is consistent with the XRD results.

Figure 5 a exhibits the circulation performance of different Fe content samples at 0.1 C in 3.0–4.8 V. It is clear that the discharge capacity of neat $Li_3V_2(PO_4)_3$ after 20 cycles was only 85 mAh g^{-1}. The Fe-doped samples have a higher capacity than pure $Li_3V_2(PO_4)_3$ due to the incorporation of Fe^{3+} which improved electrical conductivity and structural stability. The 1% sample presents the highest discharge capacity of 180 mAh g^{-1} and the retention is 91.4%. In comparison with the 1% sample, the 2% sample shows a lower capacity with poor capacity retention. Due to too much Fe^{3+} substitution in $Li_3M_2(PO_4)_3$ lattice, the closet bond lengths of Li_1–O, Li_2–O, and Li_3–O contacts are significantly reduced. The binding interaction between O and Li gradually increases, reducing the insertion/extraction mobility of lithium ions during discharge/charging [35, 36]. Therefore, with the increase in Fe amount, an excess of Fe^{3+} in the $Li_3V_2(PO_4)_3$ lattice decreases the electrochemical activities and contributes to the lower electrochemical properties of the electrodes. Figure 5b shows the rate performance of the samples at different rates increasing from 0.5 to 10 C and then reducing to 0.5 C each 5 cycles. It obviously shows that the discharge capacity is decreased as the current rate increases which indicates the electrochemical activities of $Li_3V_2(PO_4)_3$ is determined by ion diffusion. And the 1% sample electrode possesses the capacity of 145, 138, 125, 88, and 143 mAh g^{-1} at 0.5 C, 1 C, 2 C, 5 C, 10 C, and 0.5 C, respectively.

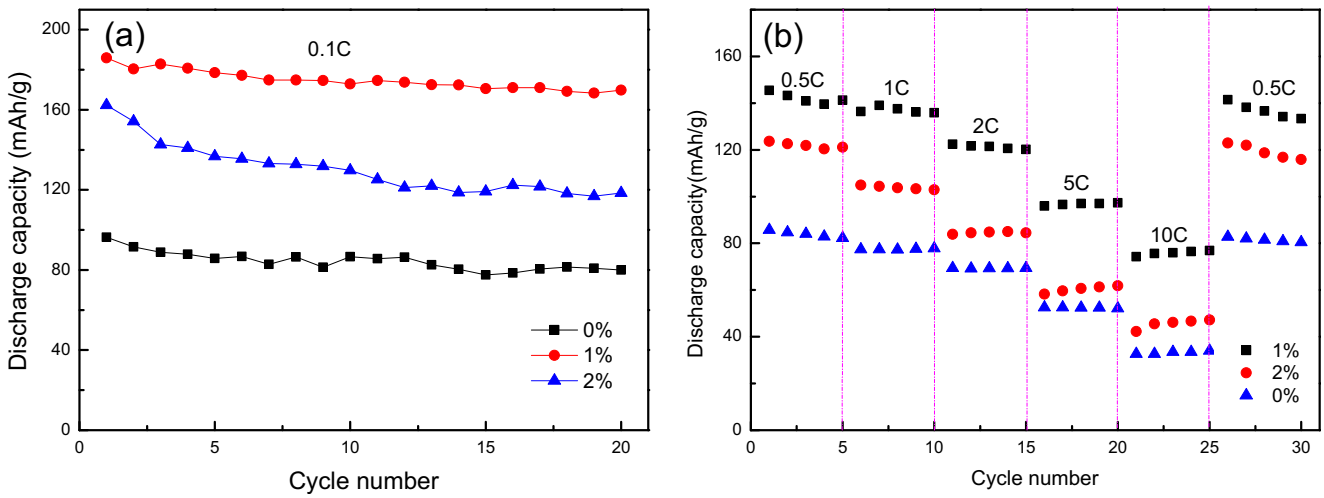

Fig. 5 **a** The resulting cycling data versus capacity for the samples (at a rate of 0.1 C between 3.0–4.8 V). **b** Comparison of the cycling performances versus C-rates

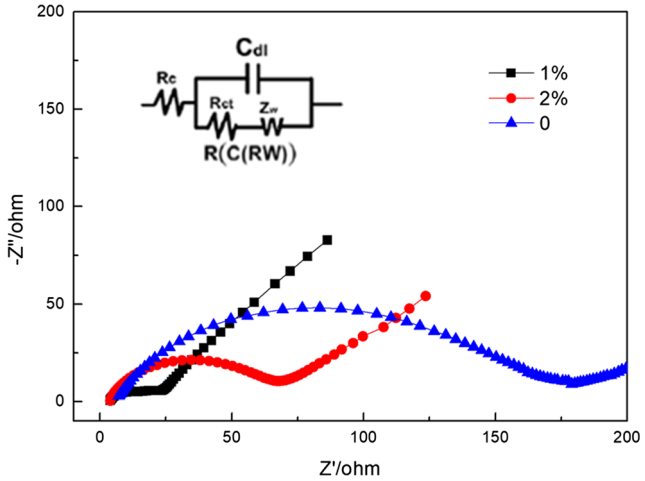

Fig. 6 Nyquist plots of the two electrodes in the frequency range of 100 kHz to 10 mHz

EIS measurements can reveal diffusion process information during charge/discharge process [37]. The kinetic properties of undoped and Fe-doped samples were studied by EIS. Figure 6 presents the Nyquist plots of all the three $Li_3V_2(PO_4)_3$ electrodes, and each plot composed of a small intercept at high frequency (corresponding to the ohm resistance of electrolyte (Re)), a depressed semicircle at medium frequency (including the charge transfer resistance between the electrode and electrolyte interface (Rct) and the double-layer capacitance between electrolyte and electrode (Cdl)), and a linear part at low frequency (associated with the Warburg resistance Zw) [38, 39]. It is obvious that the 1% Fe-doped sample shows the lowest Rct. The result is in good agreement with the electrochemical performance obtained in Fig. 5. The improvement is due to the appropriate Fe doped into the $Li_3V_2(PO_4)_3$ crystal lattice which can increase the degree of disorder in the lattice and enhance the electronic transfer conductivity.

To further study the electrochemical reaction during cycles, the CV curves of the 1% sample electrode in 3.0–4.8 V at a scanning rate of 0.1 mV s^{-1} are presented in Fig.7. Because of formation and structure rearrangement of the solid electrolyte interface (SEI) film, the CV curves were tested after five cycles[40-41]. The curves present four oxidation peaks and three reduction peaks. The oxidation peaks located at ~3.63 (A_1) and 3.72 V (A_2) are corresponding to the first Li^+ extraction from $Li_3V_2(PO_4)_3$ in two steps ascribed to the ordered phase at mixed V^{3+}/V^{4+}, and the third anodic peak (A_3) about 4.13 V is attribute to the second Li^+ extraction from $Li_2V_2(PO_4)_3$ [42-44]. The first two Li^+ extractions related to the V^{3+}/V^{4+} couple. The fourth oxidation peak (A_4) at about 4.63 V generates by the removal of the third Li^+ ($LiV_2(PO_4)_3 \rightarrow V_2(PO_4)_3$), which attributed to the V^{4+}/V^{5+} couple [1]. The border shape with lower densities of peak A_4 is ascribed to the lower electronic/ionic conductivity of $V_2(PO_4)_3$, and, therefore, it has slower reaction kinetics and lower electrochemical activity. Moreover, the peak around B_3 is due to the insertion of two Li^+ into $V_2(PO_4)_3$ by a solid solution process, which is ascribed to the V^{5+}/V^{4+} couple. The reduction peaks located at B_2 and B_1 are ascribed to a two-step insertion of the first Li^+ transform $Li_2V_2(PO_4)_3$ to $Li_{2.5}V_2(PO_4)_3$ and then to $Li_3V_2(PO_4)_3$, and it corresponds to the V^{4+}/V^{3+} pairs. To study the high current rate and circulation performance of the 1% sample, the electrodes in 3.0–4.8 V at different current densities for 500 cycles are shown in Fig. 7b. At the current of 1 C, 10 C, and 20 C, the initial special capacity is 175.7, 142.0, and 67.0 mAh g^{-1}, respectively, and the capacity was still 142.5, 132.5, and 65.9 mAh g^{-1} after 500 cycles, respectively. The results indicate that the material has good circulation performance. The

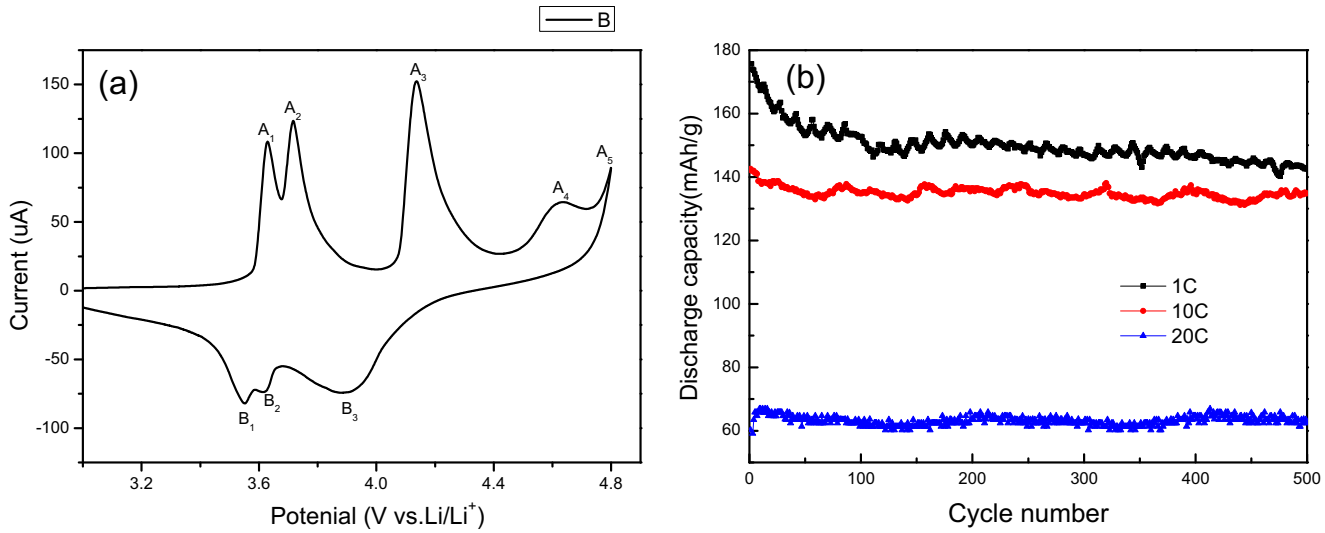

Fig. 7 **a** CV curves of 1% Fe-doped LVP/C electrodes in the potential range of 3.0–4.8 V (vs. Li^+/Li) at a scan rate of 0.1 mV/s. **b** The resulting cycling data for the samples at different rates

capacity of the cathode decreases with current rate increasing. Due to the low current density, the polarization of the electrode is also small, and the charging and discharging time is long enough for Li^+ to be inserted/extracted, so the specific capacity is higher. However, when the current density is too high, the charging and discharging time is too short, which leads to the incomplete insertion/extraction for Li^+, so the specific capacity will decrease accordingly. In general, the circulation performance of Fe-doped $Li_2V_2(PO_4)_3$ has been greatly improved.

Conclusions

Fe-doping $Li_3V_2(PO_4)_3$/C materials were successfully synthesized from combustion synthesis precursors. Because appropriate Fe doped into the $Li_3V_2(PO_4)_3$ crystal lattice which could increase the degree of disorder in lattice and enhance the electronic transfer conductivity, the 1% Fe-doped composites as cathode electrode material for LIBs exhibit enhanced electrochemical performance. In 3.0~4.8 V, it has a specific discharge capacity of 180 mAh g^{-1} at the rate of 0.1 C after 20 cycles, 142.5 mAh g^{-1} at 1 C, and 132.5 mAh g^{-1} 10 C after 500 cycles. Moreover, it shows stabilized specific discharge capacity of 65.9 mAh g^{-1} after 500 cycles at the rate of 20 C, and the capacity retention is 98%. Thus, it could infer the Fe-doping $Li_3V_2(PO_4)_3$/C material is a potential cathode material for application in LIBs with high performance. Furthermore, this work provides a new insight into the construction of cation doped $Li_3M_2(PO_4)_3$ for improving electrochemical performance.

Funding information This work was supported by the Applied Basic Research Programs of Sichuan Province (no. 2018JY0130, no. 2019JY0684) and the Applied Basic Research Programs of Panzhihua (no. 2018CY-G-11).

References

1. Sun P, Zhao X, Chen R, Chen T, Ma L, Fan Q, Lu H, Hu Y, Tie Z, Jin Z, Xu Q, Liu J (2016) $Li_3V_2(PO_4)_3$ encapsulated flexible free-standing nanofabric cathodes for fast charging and long life-cycle lithium-ion batteries. Nanoscale 8:7408–7415
2. Chen L, Yan B, Xu J, Wang C, Chao Y, Jiang X, Yang G (2015) Bicontinuous structure of $Li_3V_2(PO_4)_3$ clustered via carbon nanofiber as high-performance cathode material of Li-ion batteries. ACS Appl Mater Interfaces 7:13934–13943
3. Mao WF, Fu YB, Zhao H, Ai G, Dai YL, Meng DC, Zhang XL, Qu DY, Liu G, Battaglia VS, Tang ZY (2015) Rational design and facile synthesis of $Li_3V_2(PO_4)_3$@C nanocomposites using carbon with different dimensions for ultrahigh-rate lithium-ion batteries. ACS Appl Mater Interfaces 7:12057–12066
4. Whittingham MS (2014) Ultimate limits to intercalation reactions for lithium batteries. Chem Rev 114:1414–11443
5. Wei Q, Xu Y, Li Q, Tan S, Ren W, An Q, Mai L (2016) Novel layered $Li_3V_2(PO_4)_3$/rGO&C sheets as high-rate and long-life lithium ion battery cathodes. Chem Commun 52:8730–8732
6. Wei Q, An Q, Chen D, Mai L, Chen S, Zhao Y, Hercule KM, Xu L, Minhas-Khan A, Zhang Q (2014) One-pot synthesized bicontinuous hierarchical $Li_3V_2(PO_4)_3$/C mesoporous nanowires for high-rate and ultralong-life lithium-ion batteries. Nano Lett 14: 1042–1048
7. Kang J, Mathew V, Gim J, Kim S, Song J, Bin Im W, Han J, Lee JY, Kim J (2014) Pyro-synthesis of a high rate nano-$Li_3V_2(PO_4)_3$/C cathode with mixed morphology for advanced Li-ion batteries. Sci Rep 4:4047
8. Wang S, Zhang Z, Deb A, Yang C, Yang L, Hirano S (2014) Nanostructured $Li_3V_2(PO_4)_3$/C composite as high-rate and long-life cathode material for lithium ion batteries. Electrochim Acta 143:297–304
9. Rajagopalan R, Zhang L, Dou SX, Liu H (2016) Lyophilized 3D lithium vanadium phosphate/reduced graphene oxide electrodes for super stable lithium ion batteries. Adv Energy Mater 6:1501760
10. Liao Y, Li C, Lou X, Hu X, Ning Y, Yuan F, Chen B, Shen M, Hu B (2018) Carbon-coated $Li_3V_2(PO_4)_3$ derived from metal-organic framework as cathode for lithium-ion batteries with high stability. Electrochim Acta 271:608–616
11. Lin X, Shen Z, Han T, Liu J, Huang J, Zhou P, Zhang H, Liu J, Li J, Li J (2018) Hydrogel assisted synthesis of $Li_3V_2(PO_4)_3$ composite as high energy density and low-temperature stable secondary battery cathode. J Alloy Compd 739:837–847
12. Tang Y, Rui X, Zhang Y, Lim TM, Dong Z, Hng HH, Chen X, Yan Q, Chen Z (2013) Vanadium pentoxide cathode materials for high-performance lithium-ion batteries enabled by a hierarchical nanoflower structure via an electrochemical process. J Mater Chem A 1:82–88
13. Naoi K, Kisu K, Iwama E, Sato Y, Shinoda M, Okita N, Naoi W (2015) Ultrafast cathode characteristics of nanocrystalline-Li/carbon nanofiber composites. J Electrochem Soc 162:A827–A833
14. Kim S, Zhang Z, Wang S, Yang L, Penner-Hahn JE, De A (2018) Electrochemical and structural investigation of Mg-doped $Li_3V_{(2-2x/3)}Mg_x(PO_4)_3$. J Power Sources 396:491–497
15. Kalaga K, Sayed FN, Rodrigues MF, Babu G, Gullapalli H, Ajayan PM (2018) Doping stabilized $Li_3V_2(PO_4)_3$ cathode for high voltage, temperature enduring Li-ion batteries. J Power Sources 390: 100–107
16. Cheng Y, Feng K, Zhou W, Zhang H, Li X, Zhang H (2015) A Bi-doped $Li_3V_2(PO_4)_3$/C cathode material with an enhanced high-rate capacity and long cycle stability for lithium ion batteries. Dalton Trans 44:17579–17586
17. Zhang Y, Su Z, Ding J (2017) Synthesis and electrochemical properties of Ge-doped $Li_3V_2(PO_4)_3$/C cathode materials for lithium-ion batteries. J Alloy Compd 702:427–431
18. Yan J, Fang H, Jia X, Wang L (2018) Copper incorporated in $Li_3V_2(PO_4)_3$/C cathode materials and its effects on high-rate Li-ion batteries. J Alloy Compd 730:103–109
19. Park J, Kim J, Park WB, Sun Y, Myung S (2017) Effect of Mn $Li_3V_{2-x}Mn_x(PO_4)_3$ as high capacity cathodes for lithium batteries. ACS Appl Mater Interfaces 9:40307−40316
20. Liu X, Zhao Y, Kuang Q, Li X, Dong Y, Jing Z, Hou S (2016) Mixing transition-metal phosphates $Li_3V_{2-x}Fe_x(PO_4)_3$ ($0 \le x \le 2$): the synthesis, structure and electrochemical properties. Electrochim Acta 196:517–526
21. Varma A, Mukasyan AS, Rogachev AS, Manukyan KV (2016) Solution combustion synthesis of nanoscale materials. Chem Rev 116:14493–14586
22. Manukyan KV, Chen YS, Rouvimov S, Li P, Li X, Dong S, Liu X, Furdyna JK, Orlov A, Bernstein GH, Porod W, Roslyakov S, Mukasyan AS (2014) Ultrasmall α-Fe_2O_3 superparamagnetic

nanoparticles with high magnetization prepared by template-assisted combustion process. J Phys Chem C 118:16264
23. Cao Z, Qin M, Zuo C, Gu Y, Jia B (2017) Facile route for synthesis of mesoporous graphite encapsulated iron carbide/iron nanosheet composites and their electrocatalytic activity. J Colloid Interface Sci 491:55–63
24. Cui K, Hu S, Li Y (2016) Nitrogen-doped graphene nanosheets decorated $Li_3V_2(PO_4)_3$/C nanocrystals as high-rate and ultralong cycle-life cathode for lithium-ion batteries. Electrochim Acta 210: 45–52
25. Zhang LL, Liang G, Peng G, Jiang Y, Fang H, Huang YH, Croft MC, Ignatov A (2013) Evolution of electrochemical performance in $Li_3V_2(PO_4)_3$/C composites caused by cation incorporation. Electrochim Acta 108:182–190
26. Li Q, Wen Z, Fan C, Zeng T, Han S (2018) Chemical reaction characteristics, structural transformation and electrochemical performances of new cathode $LiVPO_4F$/C synthesized by a novel one-step method for lithium ion batteries. RSC Adv 8:7044–7054
27. Wang C, Guo Z, Shen W, Zhang A, Xu Q, Liu H, Wang Y (2015) Application of sulfur-doped carbon coating on the surface of $Li_3V_2(PO_4)_3$ composites to facilitate Li-ion storage as cathode materials. J Mater Chem A 3:6064–6072
28. Wang C, Shen W, Liu H (2014) Nitrogen-doped carbon coated $Li_3V_2(PO_4)_3$ derived from a facile in situ fabrication strategy with ultrahigh-rate stable performance for lithium-ion storage. New J Chem 38:430–436
29. Si Y, Su Z, Wang Y, Ma T, Ding J (2015) Improved electrochemical properties of (1- x)LiFePO4$x $Li_3V_2(PO_4)_3$/C composites prepared by a novel sol-gel method. New J Chem 39:8971–8977
30. Morgan D, Ceder G, Saidi MY, Swoyer J, Huang H, Adamson G (2002) Experimental and computational study of the structure and electrochemical properties of $Li_xM_2(PO_4)_3$ compounds with the monoclinic and rhombohedral structure. Chem Mater 14:4684–4693
31. Yue Y, Liang H (2017) Micro- and nano-structured vanadium pentoxide (V_2O_5) for electrodes of lithium-ion batteries. Adv Energy Mater 7:1602545
32. Cao Z, Qin M, Jia B, Gu Y, Chen P, Volinsky AA, Qu X (2015) One pot solution combustion synthesis of highly mesoporous hematite for photocatalysis. Ceram Int 41:2806–2812
33. Deshpande K, Mukasyan A, Varma A (2004) Direct synthesis of iron oxide nanopowders by combustion approach: reaction mechanism and properties. Chem Mater 16:4896–4904
34. Cao Z, Qin M, Jia B, Zhang L, Wan Q, Wang M, Volinsky AA, Qu X (2014) Facile route for synthesis of mesoporous Cr_2O_3 sheet as anode materials for Li-ion batteries. Electrochim Acta 139:76–81
35. Patoux S, Wurm C, Morcretta M, Rousse G, Masquelier C (2003) A comparative structural and electrochemical study of monoclinic $Li_3Fe_2(PO_4)_3$ and $Li_3V_2(PO_4)_3$. J Power Sources 119–121:278–284
36. Zhang LL, Sun HB, Yang XL, Li M, Li Z, Ni SB, Tao HC (2016) Natural graphite enhanced the electrochemical performance of $Li_3V_2(PO_4)_3$ cathode material for lithium ion batteries. J Solid State Electrochem 20:311–318
37. Zhang L, Li Z, Yang X, Ding X, Zhou Y, Sun H, Tao H, Xiong L, Huang Y (2017) Binder-free $Li_3V_2(PO_4)_3$/C membrane electrode supported on 3D nitrogen doped carbon fibers for high-performance lithium-ion batteries. Nano Energy 34:111–119
38. Wu J, Xu M, Tang C, Li G, He H, Li CM (2018) F-doping effects on carbon-coated $Li_3V_2(PO_4)_3$ as a cathode for high performance lithium rechargeable batteries: combined experimental and DFT studies. Phys Chem Chem Phys 20:15192–15202
39. Kim S, Zhang ZX, Wang SL, Yang L, Cairns EJ, Penner-Hahn JE, Deb A (2016) Electrochemical and structural investigation of the mechanism of irreversibility in $Li_3V_2(PO_4)_3$ cathodes. J Phys Chem C 120:7005–7012
40. Sun HB, Zhang LL, Yang XL, Huang YH, Li Z, Zhou YX, Ding XK, Liang G (2016) Effect of Fe-doping followed by C+SiO_2 hybrid layer coating on $Li_3V_2(PO_4)_3$ cathode material for lithium-ion batteries. Ceram Int 42:16557–16562
41. Saidi MY, Barker J, Huang H, Swoyer JL, Adamson G (2003) Performance characteristics of lithium vanadium phosphate as a cathode material for lithium-ion batteries. J Power Sources 119: 266–272
42. Yin SC, Grondey H, Strobel P, Anne M, Nazar LF (2003) Electrochemical property: structure relationships in monoclinic $Li_{3-y}V_2(PO_4)_3$. J Am Chem Soc 125:10402–10411
43. Ren MM, Zhou Z, Li YZ, Gao XP, Yan J (2006) Preparation and electrochemical studies of Fe-doped $Li_3V_2(PO_4)_3$ cathode materials for lithium-ion batteries. J Power Sources 162:1357–1362
44. Li Z, Zhang LL, Yang XL, Sun HB, Huang YH, Liang G (2016) Superior rate performance of $Li_3V_2(PO_4)_3$ co-modified by Fe-doping and RGO-incorporation. RSC Adv 6:10334–10340